

Atmospheric correction of GeoEye-1 images using MODIS-based parameters

Daniel Gomes¹
Ramon Felipe Bicudo da Silva²
Luiz Eduardo Vicente¹
Daniel de Castro Victoria¹

¹ Embrapa Monitoramento por Satélite
Av. Soldado Passarinho, 303. CEP 13070-115 Campinas, SP, Brazil
{daniel.gomes, luiz.vicente, daniel.victoria}@embrapa.br

² Universidade Estadual de Campinas / Núcleo de Estudos e Pesquisas Ambientais
Cidade Universitária Zeferino Vaz. CEP 13083-970 Campinas, SP, Brazil
ramonbicudo@gmail.com

Abstract. Atmospheric correction is a very important task that allows comparisons between image-based biophysical estimates and existing spectral libraries. Atmospheric correction methods based on radiative transfer provide good results as they account for scattering and absorption components effects of atmosphere over electromagnetic radiation, but the lack of ground-daily information of atmospheric parameters for radiative transfer-based models limits these methods operation. Our objective was to perform atmospheric correction of GeoEye-1 images using MODIS-based parameters as input data for the Moderate-Resolution Atmospheric Radiative Transfer Model (MODTRAN) code. That was achieved using aerosol optical thickness, Ångström exponent, and water column data extracted from MODIS Aqua data in order to obtain visibility, aerosol scale height, and atmospheric model to be used in MODTRAN. The results were analyzed from a set of pixels arranged in six land cover classes that were compared to the spectral libraries USGS and NASA/JPL, available online. Land cover classes of pasture, urban areas, forest, dark soil, medium soil, and light soil presents satisfactory combinations by the Spectral Angle Mapper method, used to compare spectra from the GeoEye-1 images and spectral libraries. We conclude that the methodological approach presented is a promising standard of methods based on the retrieving of atmospheric information to perform radiometric corrections.

Keywords: radiative transfer, visibility, aerosol scale height, transfrência radiativa, visibilidade, altura de escala do aerossol.

1. Introduction

Remote sensing is a technique widely used for earth surface components examination. However, additive and multiplicative effects from the atmosphere over electromagnetic radiation hamper target identification in satellite images. Atmospheric correction reduces this difficulty, and allows estimating biophysical characteristics from the targets, using satellite imagery data (Vicente and Souza Filho, 2011).

Radiative transfer-based atmospheric correction models simulate the propagation of sun electromagnetic radiation through the atmosphere and have the advantage of correcting atmospheric scattering and absorption components effects (Ju et al., 2012). Even though radiative transfer-based models solve these issues, they require specific atmospheric characterization from the imaged area at the exact time of scenes acquisition, which is often not available for all locations (Gomes et al., 2013; Ju et al., 2012; Vermote et al., 2002).

The Moderate-Resolution Atmospheric Radiative Transfer Model code (MODTRAN) performs atmospheric correction of images and is able to estimate a wide variety of parameters it needs to correct the images (Adler-Golden et al., 1999). But MODTRAN estimates are based on spectral characteristics of the image to be corrected. Though, if the image do not have bands in the shortwave infrared channel around 2.1 micrometers (μm), for example, MODTRAN cannot estimate the image visibility or the aerosol amounts that affects the atmospheric scattering of electromagnetic radiation (Research Systems Inc., 2005; Kaufman et al., 1997).

GeoEye-1 satellite produces images with spatial resolution of 2 m in its four multispectral bands and has radiometric resolution of 11 bits per pixel per band. However, GeoEye-1 does not measure radiation at 2.1 μm (Arnold et al., 2013), thus it cannot generate intrinsic estimates of aerosol amounts in order to perform atmospheric correction of its images.

The Moderate-Resolution Imaging Spectroradiometer sensor (MODIS) onboard Aqua and Terra satellites is able to retrieve aerosols data by a combination of its spectral reflectance data and the simulations of optical models of aerosols conditions registered in lookup tables (Remer et al., 2005). Beyond that, MODIS data are distributed not only as raw data, but also in thematic products developed to take advantage of MODIS near-daily observations repeatability at global scales (Remer et al., 2005). These products include the Giovanni portal, a website that permits visualization and retrieval of atmospheric parameters not only from MODIS, but also from many sources of information (Acker and Leptoukh, 2007). MODIS atmospheric data quality allows the use of its information as a basis to perform atmospheric correction of other images (Gomes et al., 2013).

In this context, our objective is to propose the use of MODIS atmospheric products data in order to obtain input parameters for atmospheric correction of GeoEye-1 images. The method we present here was previously tested in Landsat TM images (Gomes et al., 2013), and continues our efforts in getting thorough atmospheric correction of images acquired in tropical regions, where atmospheric characterization data is not systematically available.

2. Methodology

The study area comprises two GeoEye-1 images taken in the northwestern region of São Paulo State, Brazil (Fig. 1). Each image is the result of composition between five scenes acquired from October 24th 2013 to November 11th 2013. GeoEye-1 imagery has spatial resolution of 0.5 m in panchromatic band, and of 2.0 m in the multispectral bands. The spectral bands are: blue (0.45 – 0.51 μm), green (0.51 – 0.58 μm), red (0.655 – 0.69 μm) and near infrared (0.78 – 0.92 μm). at a quantization level of 11 bits per pixel per band (Arnold et al., 2013).

We transformed digital numbers values of both images to radiance values using Arnold et al. (2013) method. Then, we used the radiance images as input data to run MODTRAN atmospheric correction. MODTRAN is able to correct images using water vapour estimates, elevation data, visibility estimates and spectral polishing method (Adler-Golden et al., 1999).

Nevertheless, the atmospheric data that MODTRAN needs to perform atmospheric correction are very difficult to be obtained during image acquisition time. We overcame this issue using MODIS Aqua data retrieved from NASA Giovanni portal (Acker and Leptoukh, 2007) available online at <http://disc.sci.gsfc.nasa.gov/giovanni>. Giovanni MODIS Aqua aerosol optical thickness and Ångström exponent data from October 24th 2013 were used to estimate initial visibility (V) to both images, using Equation 1 (Gomes et al., 2013; Ponzoni et al., 2007; Deschamps et al., 1981):

$$V = \left| (-15) \ln \left(\frac{\tau_{a(\lambda)} \lambda^\alpha}{0.613} \right) \right| \quad (1)$$

where λ is wavelength in micrometers (μm), defined as 0.55 μm in MODIS data, $\tau_{a(\lambda)}$ is aerosol optical thickness at 0,55 μm , retrieved from Giovanni MODIS Aqua data, and α is Ångström exponent also retrieved from Giovanni MODIS Aqua data.

Aerosol scale height (z_a) values are retrieved according to Equation 2 (Gomes et al., 2013; Wong et al., 2009):

$$z_a = \frac{V * \tau_{a(\lambda)}}{3.912} \quad (2)$$

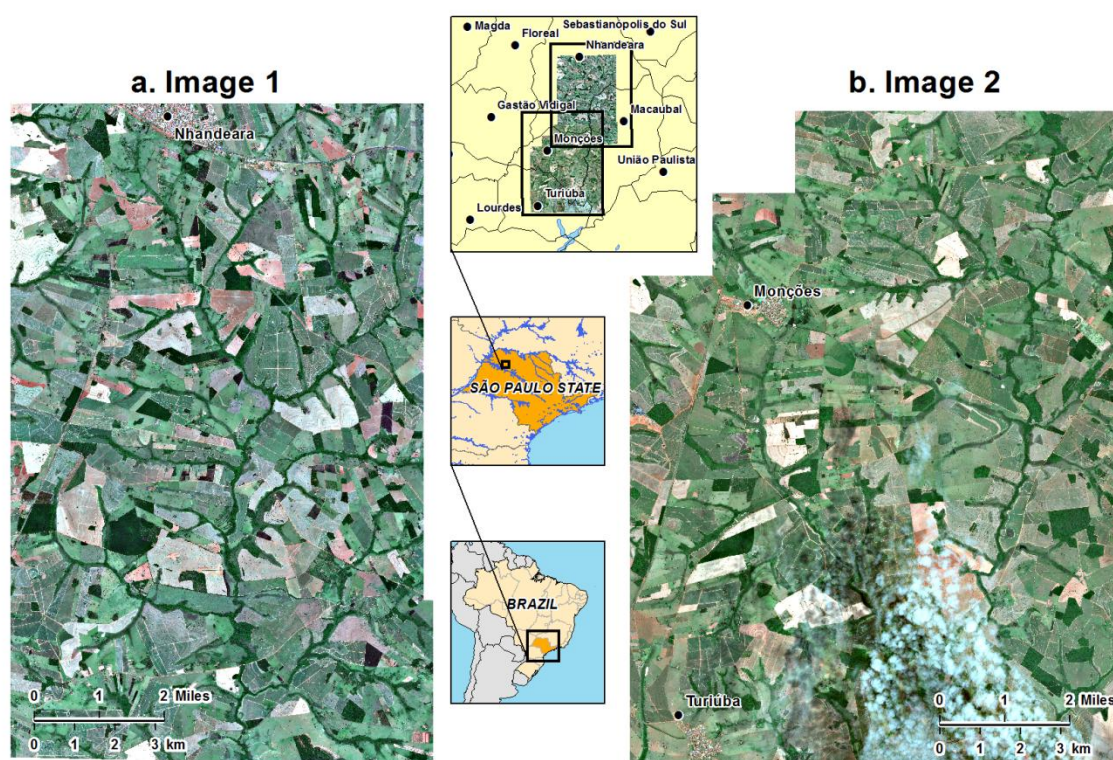


Figure 1. Study area contextualization and GeoEye-1 images used in this work.

We selected MODTRAN atmospheric model according to the water vapour values obtained from Giovanni MODIS Aqua data, as described in Gomes et al. (2013) and in Research Systems Inc. (2005).

All these calculations can be performed in Embrapa's Laboratory of Spectroradiometry (Labspec) site, available online at <http://mapas.cnpm.embrapa.br/labspec>, where users can sign up, choose image coordinates, and acquisition time in order to obtain MODTRAN parameters and perform atmospheric correction.

Field measurements were not available to validate atmospheric correction. Then, in order to discuss the results, we analyzed similarities between the mean spectra of seven land cover classes in both images and reference spectra obtained from Aster Spectral Library, available online at <http://speclib.jpl.nasa.gov/>, and USGS Digital Spectral Library, available at <http://speclab.cr.usgs.gov/spectral.lib06> (Baldrige et al., 2006; Clark et al, 2007). The most evident land covers selected in the images were: pasture, forest, urban area, water and 3 different classes of soil, according to their colors. We chose the Spectral Angle Mapper (SAM) algorithm for spectral analysis due to its sensitivity and capability of non-illuminated pixel analysis (Kruse et al., 1993). As SAM values are inversely proportional to reference and test spectra similarity, we modified the index in order to avoid counter-intuitive interpretations, using the Equation 3:

$$SAM_{adjusted} = 1 - SAM \quad (3)$$

3. Results and discussion

The lack of field measurements leads us to analyze the atmospheric correction results by comparing the corrected image spectra with reference spectra obtained from USGS and NASA/JPL (Clark et al, 2007; Baldrige et al., 2006). For each class, table 1 shows $SAM_{adjusted}$ values for all reference spectra that reach a minimum of 0.9 in the two GeoEye-1

corrected images. For pasture areas, $SAM_{adjusted}$ minimum threshold value is lowered to 0.8, since maximum $SAM_{adjusted}$ in this class is 0.867. Water class spectrum has no good correspondence with any reference spectra, as shown in table 1 and fig. 2d, thus we show only the reference spectrum with better correspondence to water spectrum. It is important to highlight that $SAM_{adjusted}$ values are not determined only by spectral similarity between spectral data, but also by the projection of shadow effects over spectral signature (Kruse et al., 1993).

$SAM_{adjusted}$ maximum value of 0.867 for pasture class correspondence with reference spectra is due to high mixture levels between soil and vegetation components in pasture areas. The best-fit to pasture class spectra is a reference spectrum measured from a whole specimen of rabbitbrush (*Chrysothamnus nauseosus*), leaves and stems included. The presence of stems in reference spectrum sample produces attenuation in visible spectrum absorption feature and in near infrared reflectance increase typical to green foliage reflectance (Asner, 2004).

Table 1. $SAM_{adjusted}$ values for each reference spectra per land cover class in GeoEye-1 atmospherically corrected images.

Class	Reference Spectrum	$SAM_{adjusted}$		
		Image1	Image2	Avg
Pasture	<i>Rabbitbrush ANP92-27</i>	0.867	0.867	0.867
	Olive green paint 0407	0.831	0.825	0.828
	Cuprite HS 127.3B	0.813	0.837	0.825
	Olive green paint 0408	0.821	0.820	0.821
Forest	<i>Lawn Grass GDS91 (Green)</i>	0.993	0.910	0.952
	Blackbrush ANP92-9A leaves	0.931	0.965	0.948
	Maple Leaves DW92-1	0.973	0.921	0.947
	Aspen Leaf-B DW92-3	0.950	0.938	0.944
	Pinon Pine ANP92-14A needle	0.909	0.961	0.935
	Aspen Leaf-A DW92-2	0.915	0.947	0.931
Urban Area	<i>Paleustalf 87P473 (Dark reddish brown fine sandy loam)</i>	0.976	0.915	0.946
	Grossular NMNH 155371	0.927	0.962	0.945
	Spessartine HS112.3B	0.936	0.935	0.936
Water	Hypersthene PYX02.c 180um	0.402	0.000	0.201
Soil 1 (dark)	<i>Grossular NMNH 155371</i>	0.961	0.986	0.974
	<i>Paleustalf 87P473 (Dark reddish brown fine sandy loam)</i>	0.962	0.927	0.945
	Spessartine HS112.3B	0.939	0.933	0.936
	Haplustalf 87P3665 (Brown fine sandy loam)	0.943	0.900	0.922
	Sauconite GDS135	0.927	0.911	0.919
	Fragiboralf 86P1994 (Pale brown silty loam)	0.934	0.902	0.918
Soil 2 (medium)	<i>Sauconite GDS135</i>	0.936	0.965	0.951
	Siderite HS271.3B	0.945	0.950	0.948
	Grossular NMNH 155371	0.963	0.905	0.934
	<i>Paleustalf 87P473 (Dark reddish brown fine sandy loam)</i>	0.954	0.906	0.930
	Haplustalf 87P3665 (Brown fine sandy loam)	0.936	0.908	0.922
	Hematite 2%+98% Qtz GDS76	0.901	0.933	0.917
	Monazite HS255.3B	0.908	0.916	0.912
Soil 3 (light)	<i>Sphalerite S102-8</i>	0.984	0.967	0.976
	Haplustalf 87P3468 (Brown loamy fine sand)	0.978	0.957	0.968
	Haplustalf 87P3671 (Brown fine sandy loam)	0.963	0.968	0.966
	Almandine HS114.3B	0.951	0.956	0.954
	Xerumbrept 87P325 (Brown to dark brown gravelly fine sandy loam)	0.948	0.949	0.949
	Hapludult 87P707 (Brown to dark brown loamy sand)	0.933	0.958	0.946
	Nontronite SWa-1.b <2um	0.958	0.930	0.944

Class (cont.)	Reference Spectrum (cont.)	SAM _{adjusted} (cont.)		
		Image1	Image2	Avg
	Spessartine NMNH14143	0.942	0.939	0.941
	Nontronite SWa-1.a	0.945	0.924	0.935
	Tumbleweed ANP92-2C Dry	0.932	0.936	0.934
	Sphene HS189.3B	0.934	0.933	0.934
	Quartzipsamment 87P706 (Brown to dark brown sand)	0.911	0.946	0.929
	Plaggept 85P3707 (Very dark grayish brown silty loam)	0.932	0.915	0.924
	Andalusite NMNHR17898	0.900	0.940	0.920
	Haplumbrept 88P4699 (Brown sandy loam)	0.916	0.917	0.917
	Praseodymium Oxide GDS35	0.907	0.921	0.914

This attenuation is probably the reason of the similarity between this reference and pasture class spectra. Other reference spectra with high correspondence with pasture spectrum are two olive green paints signatures resembling green leaves spectral signatures, and a highly absorbing signature of the copper oxide mineral cuprite (Fig. 2a). Even if cuprite is not actually present in this scene, this result suggests that the mineral composition of the soil component background in pasture class may be dominated by highly-absorbing minerals in visible spectrum. As long as pasture class reflectance spectrum behaves as a mixture of bare soil, nonphotosintetic vegetation and green vegetation (Kaplan et al., 2014; Magiera et al., 2013), we assume that the proposed atmospheric correction generates coherent pasture reflectance data in GeoEye-1 images.

Forest spectra have better correspondence with reference spectra related to green leaves measurements, regardless of leaf size or canopy structure (Fig. 2b). The best results are in the visible bands, where reflectance values are almost the same registered in all reference spectra. The best-fit reference spectra for forest class is a generic lawn grass, which is the spectrum that possess the greater NDVI value among all reference spectra used in this analysis. Lower values for near infrared band in GeoEye-1 spectra of forest class may be related to shadow effects produced by canopy structure in some pixels of this class. This result confirms that the proposed atmospheric correction works consistently for forest class reflectance as well.

Urban area spectral analysis is a difficult task to perform due to the heterogeneity of its constituent materials (Lu et al., 2011). In our GeoEye-1 images, urban area land cover class shows dominance of soil-like materials, like bricks and rooftops, associated with asphalt, grass and trees. The spectral signature of urban area class presents soil features, so that the best-fit reference spectrum is a sample of the soil class Paleustalf, which is described as a dark reddish brown fine sandy loam (Fig. 2c). This soil class description matches the description of clays that can be used in construction materials production (Salim et al., 2014), and therefore, endorses our proposed atmospheric corrected data as credible urban area reflectance data.

Water class spectrum do not correspond well with any reference spectra used in our work, because we did not use any water reference spectrum measured in visible to short-wave infrared channels (Fig. 2d). Even though, the only fit reference spectrum is a sample of hypersthene, an orthorhombic pyroxene currently known as enstatite, that gets an average SAM_{adjusted} value of 0.210. Hypersthene spectrum matches only with water spectrum of GeoEye-1 image 1, and this match probably occurred because water spectrum resembles poorly a shadow spectrum of hypersthene. Water class spectra in both images show bad results in near infrared channel, with reflectance developing negative values. Consequently, this result leads us to consider that the proposed atmospheric correction is not working properly for water reflectance data in GeoEye-1 images.

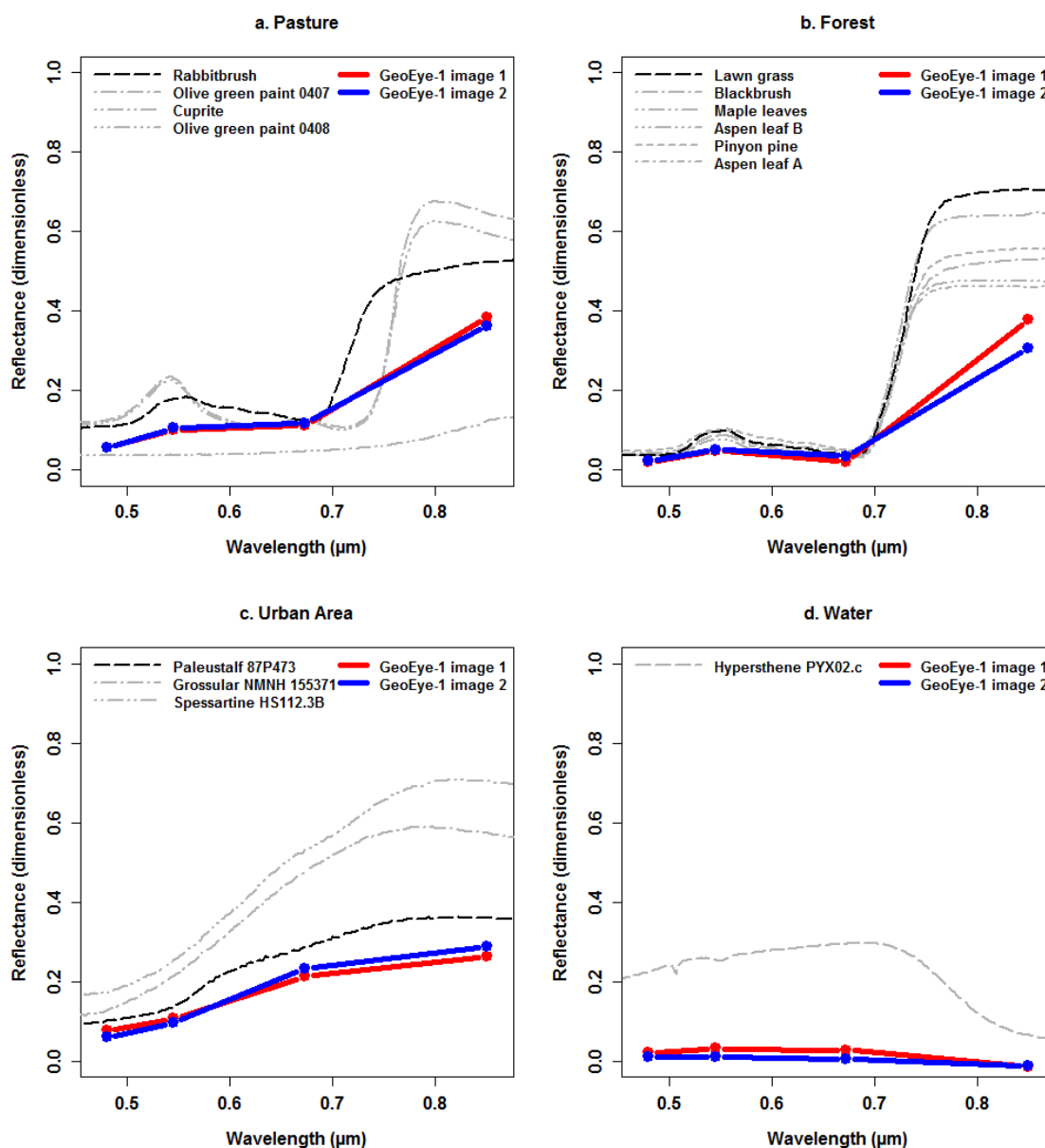


Figure 2. Spectral signature for GeoEye-1 corrected images and best-fit reference spectra determined by $SAM_{adjusted}$ for land cover classes with no bare soil fraction dominance. Thick black lines are reference spectra with the best $SAM_{adjusted}$ value of each class.

Both spectral libraries we used as reference have many examples of minerals and soils spectra due to the high sensitivity and variability of their spectral features. We could not take full advantage of this variability in our analysis because part of these features occurs in infrared spectral channels out of GeoEye-1 images spectral reach, or because some of these features are spectrally too narrow to be detected in GeoEye-1 imagery. Consequently, $SAM_{adjusted}$ analysis results for soil classes are very wide, indicating up to sixteen different reference spectra as correspondent to the soils classes. Nevertheless, these “best-fit” reference spectra are intrinsically coherent and converge to similar results in all three classes of soil.

Most of reference spectra related to GeoEye-1 soil classes show spectral characteristics that resemble tropical oxisols reflectance in visible and near infrared channels, even in the case of minerals not related with oxisols. The most evident feature is a strong wide absorption band in blue to green channel, which indicates the presence of iron oxides which are common

in tropical soils. Moreover, a simple visual analysis of Fig. 3 leads us to conclude that most of reference spectra related to a same soil class can be considered as spectral shadows variants from each other. This shadow-like similarity is evident even in monazite spectrum related to soil class 2, taking into account that the spectral absorption bands that monazite displays in visible and infrared channels are too narrow to affect GeoEye-1 bands reflectance.

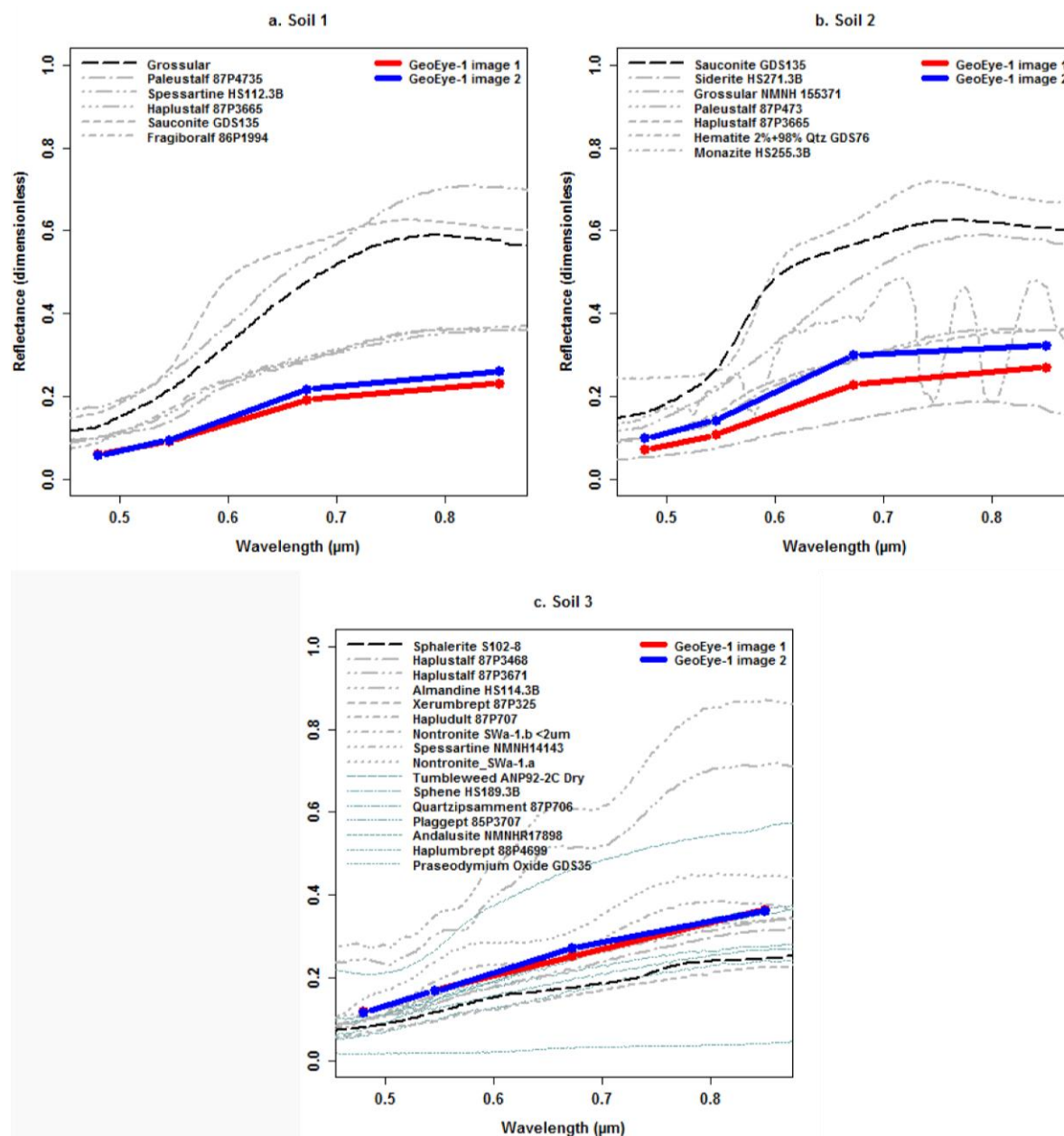


Figure 3. Spectral signature for GeoEye-1 corrected images and best-fit reference spectra determined by SAM_{adjusted} for land cover classes with bare soil fraction dominance. Thick black lines are reference spectra with the best SAM_{adjusted} value of each soil class.

Additionally, reference spectra assigned as best-fit to each class of soil are consistent with the soil class spectral signature format: soil class 2 spectral signature has more marked absorption band in 0.5 – 0.55 μm channel; in soil class 1, the same absorption band is smoother than in soil 2 class; and in soil class 3 this absorption band is nearly indistinguishable. It is worth highlighting that the only non-mineral spectrum correspondent to the soil classes is a dried tumbleweed spectrum analogous to white-colored soil class 3. In

this context, we can conclude that our atmospheric correction methodology generates consistent spectral data to soil spectra in GeoEye-1 imagery.

3. Conclusions

We applied MODTRAN atmospheric correction in two GeoEye-1 sets of images, using parameters derived from MODIS-Aqua atmospheric products. Despite the lack of field validation, we demonstrate that this atmospheric correction approach generates reliable reflectance data for different land cover pixels. Spectral analysis of corrected data using USGS and NASA/JPL reference libraries as ground truth data shows that spectra of pasture class in GeoEye-1 present adequate correspondence with whole-plant rabbitbrush spectrum and with cuprite spectrum, indicating a mixture of soil and vegetation fractions, typical of pasture areas. Spectra of corrected forest pixels are extremely similar to green leaves reference spectra, and have excellent correspondence to reference spectra reflectance in visible channels. Urban area spectra demonstrate similarity with soil reference spectra, because of the composition of rooftop tiles. And soil spectra match with a wide range of soil and minerals reference spectra intrinsically coherent and related to tropical oxisols reflectance spectra. Water spectra represent the only land cover class that generates poor results in its reflectance spectrum.

Acknowledgements

We acknowledge the team of the project “Multisensor data integration and reflectance spectroscopy applied to strategic targets mapping of tropical agriculture” project (Embrapa - 02.11.01.019.00.00), regarding to financial and technical support.

References

- Acker, J. G.; Leptoukh, G. Online analysis enhances use of NASA Earth Science data. **Eos**, Transactions AGU, v. 88, n. 2, p. 14-17, 2007.
- Adler-Golden, S. M.; Matthew, M. W.; Bernstein, L. S.; Levine, R. Y.; Berk, A.; Richtsmeier, S. C.; Acharya, P. K.; Anderson, G. P.; Felde, G. W.; Gardner, J. A.; Hoke, M. L.; Jeong, L. S.; Pukall, B.; Ratkowski, A.; Burke, H.-H. Atmospheric correction for short-wave spectral imagery based on MODTRAN. In: SPIE Imaging Spectrometry, 5., 1999. **Proceedings ...** v. 3753, 9 p. 1999.
- Arnold, R.; Podger, N.; Seidler, E. GeoEye-1 stellar radiometric calibration. In: Annual JACIE (Joint Agency Commercial Imagery Evaluation) Workshop, 12., April 16-18, 2013, St. Louis, MO, USA. **Proceedings...** St. Louis: JACIE, 2013. URL: <<http://www.genesiis.com/pdf/GeoEye-1-parameters.pdf>>
- Asner, G. P. Biophysical remote sensing signatures of arid and semiarid ecosystems. In: Ustin, S. L. (Ed.) **Remote sensing for natural resource management and environmental monitoring**. Manual of remote sensing, v. 4. Hoboken: John Wiley & Sons / American Society for Photogrammetry and Remote Sensing, 2004. Chapter 2, p. 53-109.
- Baldrige, A. M.; Hook, S. J.; Grove, C. I.; Rivera, G. The ASTER Spectral Library Version 2.0. **Remote Sensing of Environment**, v. 113, p. 711-715, 2009.
- Clark, R. N.; Swayze, G. A.; Wise, R.; Livo, E.; Hoefen, T.; Kokaly, R.; Sutley, S. J. **USGS digital spectral library splib06a**: U.S. Geological Survey, Digital Data Series 231. 2007.

- Deschamps, P. Y.; Herman, M.; Tanré, D. Influence de l'atmosphère en télédétection des ressources terrestres: modélisation et possibilités de correction. In: Colloque de la Société Internationale de Photogrammétrie et de Télédétection, September, 1981, Avignon, France. **Proceedings...** Avignon: ISPRS, 1981, p. 543-558.
- Gomes, D.; Vicente, L. E.; Silva, R. F. B.; Paula, S. C.; Maçorano, R. P.; Victoria, D. C.; Batistella, M. Uso de dados MODIS e AIRS para obtenção de parâmetros de correção atmosférica. In: Simpósio Brasileiro de Sensoriamento Remoto (SBSR), 16., 2013, Foz do Iguaçu. **Proceedings ...** São José dos Campos: INPE, 2013. Artigos, p. 8019-8026.
- Ju, J.; Roy, D. P.; Vermote, E.; Masek, J.; Kovalsky, V. Continental-scale validation of MODIS-based and LEDAPS Landsat ETM+ atmospheric correction methods. **Remote Sensing of Environment**, v. 122, p. 175-184, 2012.
- Kaplan, S.; Blumberg, D. G.; Mamedov, E.; Orlovsky, L. Land-use change and land degradation in Turkmenistan in the post-Soviet era. **Journal of Arid Environments**, v. 103, p. 93-106, 2014.
- Kaufman, Y. J.; Wald, A. E.; Remer, L. A.; Gao, B.; Li, R.; Flynn, L. The MODIS 2.1- μm channel—correlation with visible reflectance for use in remote sensing of aerosol. **Transactions on Geosciences and Remote Sensing**, v. 35, n. 5, p. 1286-1298, 1997.
- Kruse, F. A.; Lefkoff, A. B.; Boardman, J. B.; Heidebrecht, K. B.; Shapiro, A. T.; Barloon, P. J.; Goetz, A. F. H. The Spectral Image Processing System (SIPS) - interactive visualization and analysis of imaging spectrometer data. **Remote Sensing of Environment**, Special issue on AVIRIS, v. 44, p. 145-163, 1993.
- Lu, D.; Moran, E.; Hetrick, S. Detection of impervious surface change with multitemporal Landsat images in an urban–rural frontier. **ISPRS Journal of Photogrammetry and Remote Sensing**, v. 66, p. 298-306, 2011.
- Mariega, A.; Feihauer, H.; Otte, A.; Waldhardt, R.; Simmering, D. Relating canopy reflectance to the vegetation composition of mountainous grasslands in the Greater Caucasus. **Agriculture Ecosystems & Environment**, v. 177, p. 101-112, 2013.
- Ponzoni, F. J.; Zullo Jr., J.; Lamparelli, R. A. C. **Calibração absoluta de sensores orbitais: conceituação, principais procedimentos e aplicação.** São José dos Campos, SP: Editora Parêntese, 2007. 80 p.
- Remer, L. A.; Kaufman, Y. J.; Tanré, D.; Mattoo, S.; Chu, D. A.; Martins, J. V.; Li, R. –R.; Ichoku, C.; Levy, R. C.; Kleidman, R. G.; Eck, T. F.; Vermote, E.; Holben, B. N. The MODIS Aerosol Algorithm, Products, and Validation. **Journal of Atmospheric Sciences**, v. 62, p. 947-973, 2005.
- Research Systems Inc. FLAASH Module User's Guide. In: **IDL Assistant**, 2005.
- Salim, R. W.; Ndambuki, J. M.; Adedokun, D. A. Improving the bearing strength of sandy loam soil compressed earth block bricks using sugarcane bagasse ash. **Sustainability**, v. 6(6), p. 3686-3696, 2014.
- Vermote, E. F.; El Saleous, N.; Justice, C. O. Atmospheric correction of MODIS data in the visible to middle infrared: first results. **Remote Sensing of Environment**, v.83, n. 1-2, p. 97-111, 2002.
- Vicente, L.E.; Souza Filho, C.R. de. Identification of mineral components in tropical soils using reflectance spectroscopy and advanced spaceborne thermal emission and reflection radiometer (ASTER) data. **Remote Sensing of Environment**, v.115, p.1824-1836, 2011. DOI: 10.1016/j.rse.2011.02.023
- Wong M. S.; Nichol, J. E.; Lee, K. H. Modeling of aerosol vertical profiles using GIS and remote sensing. **Sensors**, v. 9, p. 4380-4389, 2009.